NASA-CR-201003

Final Report
Attachment 6

October 17, 1995

CONTRACT NAS8-38856

Structural Damage Prediction and Analysis for Hypervelocity Impact

HVIS92 049 G1 Characteristics of Debris Clouds Produced by Hypervelocity Impact of Aluminum Spheres with Thin Aluminum Sheets

Prepared for:
National Aeronautics and Space Administration
George C. Marshall Space Flight Center
Marshall Space Flight Center,
Alabama 35812

LOCKHEED MARTIN

MAF/MMA 31-100 (3/95)

Int. J. Impact Engng Vol. 14, 1993 , p573 - 586

CHARACTERISTICS OF DEBRIS CLOUDS PRODUCED BY HYPERVELOCITY IMPACT OF ALUMINUM SPHERES WITH THIN ALUMINUM PLATES.

ANDREW J. PIEKUTOWSKI

University of Dayton Research Institute
Dayton, Ohio 45469

ABSTRACT

Debris clouds produced by the normal impact of aluminum spheres with aluminum bumper plates are shown to consist of an ejecta veil, an external bubble of debris, and a significant internal structure composed of three distinct elements. Effects of variations in bumper-plate thickness, sphere diameter, and impact velocity on the shape and velocity of the elements of the internal structure are described and compared. Three alloys of bumper material and several diameters of 2017-T4 aluminum spheres, ranging from 6.35 mm to 12.70 mm, were used in the tests described in this paper. Test results were sorted into two sets. In the first set, impact velocity was held constant at 6.7 km/s and the bumper-thickness-to-projectile-diameter ratio, t/D, varied from 0.026 to 0.424. In the second set, t/D ratio was held constant at 0.049 and the impact velocity varied from 3.77 km/s to 7.23 km/s. In both sets of test results, debris-cloud properties are shown to scale with projectile diameter. Characteristics of the front element of the debris-cloud internal structure are shown to be sensitive to changes in t/D ratio and impact velocity. A model for the formation of this front element is presented and used to develop a description of a debris cloud consisting of material in the solid-liquid and/or liquid-vapor phases.

INTRODUCTION

From earliest interest in the development of spacecraft shield systems, investigators have used a variety of materials to simulate micrometeoroids. A significant fraction of the work has employed aluminum spheres impacting aluminum sheets or plates (Maiden, 1963; Maiden et al., 1965; Backman and Stronge, 1967; Swift and Hopkins, 1968; and Nysmith and Denardo, 1969; and others). Aluminum spheres continue to be used in shield studies as simulants of orbital-debris fragments. Determination of the ballistic limit of a shield, optimization of a shield against a specific threat, and/or development of design criteria are the usual purposes for most test programs. Occasionally, radiographs or high-speed photographs of "typical" debris clouds are presented with test results. However, quantitative descriptions of the debris clouds are rarely given and when descriptions are provided, they are not systematic (i.e., did not describe changes in the debris-cloud morphology as a result of changes in impact velocity, bumper thickness, etc.)

This paper examines the formation of debris clouds produced by the impact of aluminum spheres with thin aluminum plates and presents results of tests used to quantitatively evaluate debris-cloud

morphology as a function of bumper-thickness-to-projectile-diameter ratio, t/D, and impact velocity. The evaluation was limited to: (1) t/D ratios from 0.026 to 0.424 for an impact velocity of 6.7 km/s and (2) impact velocities from 3.77 km/s to 7.23 km/s for a t/D ratio of 0.049. All impacts were normal to the bumper or front sheet. A model for the interaction and effect of shock-wave processes initiated by the impact event is presented. Finally, a description of debris clouds containing liquid and vapor is presented for the case in which the t/D ratio is near optimum.

EXPERIMENTAL DESIGN

Data presented in this paper were obtained from tests performed for Martin Marietta Manned Space Systems, McDonnell Douglas Space Systems Company, and from equipment and/or range performance tests conducted by the University of Dayton Research Institute (UDRI). All tests were performed in the UDRI Impact Physics Laboratory using a 50/20 mm, two-stage, light-gas gun.

The tests were performed with the bumper plate normal to the range center line. Various thicknesses of 1100-O, 2024-T3, and 6061-T6 aluminum plates, ranging from 0.25 mm to 4 mm, were used as bumpers. Most tests used 9.53-mm-diameter 2017-T4 aluminum spheres as their projectiles. Several tests used 6.35-mm or 12.70-mm-diameter 2017-T4 aluminum spheres. The specific plate alloy, thickness, and sphere diameter used for each test are included in figures presented later in this paper. Impact velocity for the tests ranged from 3.77 km/s to 7.23 km/s and was determined using time-of-flight measurements between four laser-photodetector stations located along the range center line. Accuracy of the impact velocity determination was better than $\pm$ 0.5 percent. Finally, an aluminum witness plate was placed 38 cm downrange of the bumper, for each test, to record the damage pattern produced by the debris cloud.

Three or four pairs of fine-source, soft, flash x-rays were used to observe the projectile and debris clouds. The x-ray heads were accurately positioned on the target chamber to provide simultaneous orthogonal views of the debris clouds. Although individual test setups varied slightly, a typical test setup for one view is shown in Fig. 1. The first pair of x-rays was used to view and record the position of the projectile a few microseconds before impact. This view served to verify projectile integrity and to permit accurate determination of the time after impact for the two or three views taken of the debris cloud after its formation. Normally, views were taken when the cloud was about 4 cm and 12 cm downrange (approximately 6 μs and 19 μs, respectively, after impact). The fourth pair of x-rays, if used, were usually not fired until the debris cloud was about 30 cm downrange of the bumper. The delay in firing the x-rays allowed the cloud to expand and permitted a more detailed

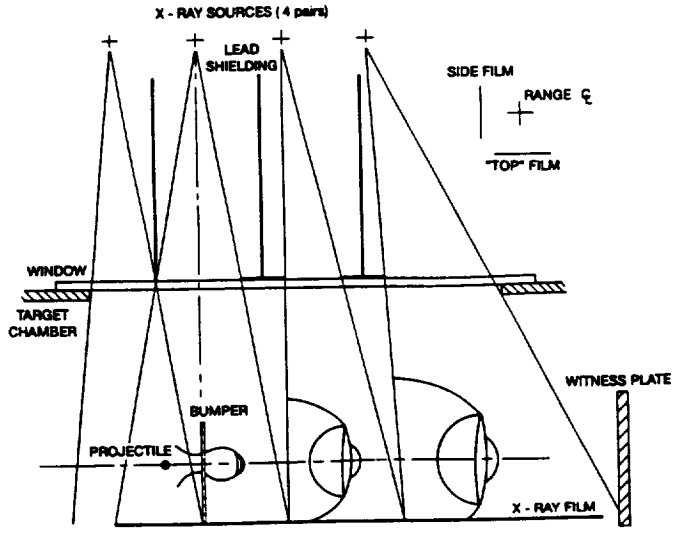

Fig. 1. Setup used to obtain multiple-exposure, orthogonal-pair, flash radiographs of debris clouds.

examination of the cloud structure. The fourth pair of heads was usually positioned as shown in Fig. 1 to obtain an oblique (~ 13 degrees from normal) view of the cloud; in some tests these heads were positioned 31.5 cm downrange of the bumper to provide a normal view of the cloud.

Post test documentation consisted of measurement of bumper-hole diameters and witness-plate damage patterns. Debris-cloud measurements taken from the radiographs and the late-time views were analyzed, when possible, to determine the largest fragment dimensions and the size and number of fragments forming the debris cloud. Results of these additional measurements may be found in Piekutowski (1992a and 1992b).

DESCRIPTION OF DEBRIS CLOUDS

Two views of a debris cloud are presented in Fig. 2 to illustrate three major features of the cloud. First, an ejecta veil, consisting almost entirely of bumper fragments, is ejected from the impact or front side of the bumper. Second, an expanding bubble of bumper debris forms on the rear side of the bumper. Finally, there is a significant structure composed of projectile debris located inside and at the front of the external bubble of bumper debris. This internal structure is composed of a front, center, and rear element. For a 6.70 km/s impact, the front element consists of finely divided,

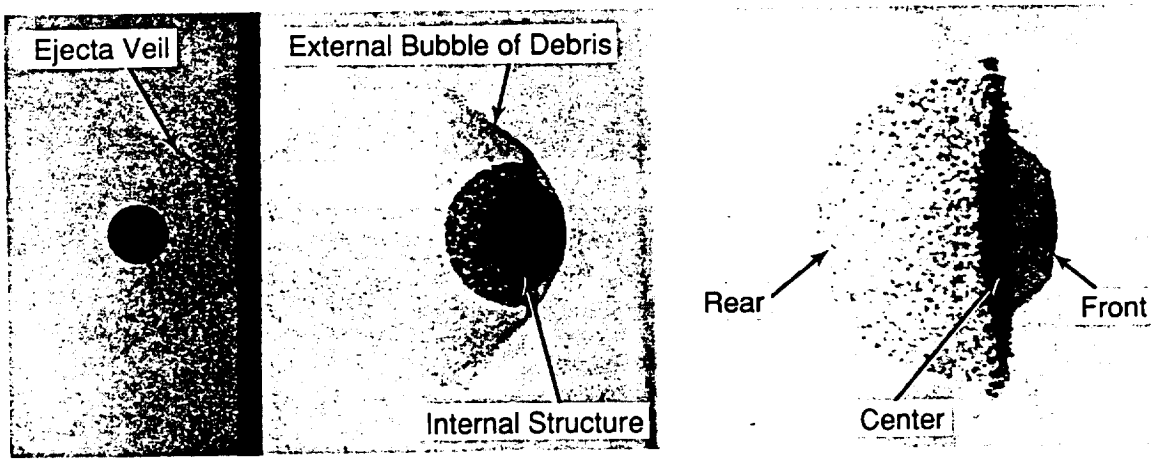

Fig. 2. Morphological features and elements of a debris cloud. Note that the ejecta veil and projectile are a double exposure in this figure and in all radiographs presented in this paper.

molten droplets of bumper and projectile. The center disc-like element is composed of numerous splintery projectile fragments. This element also contains a single large chunky projectile fragment that is located at the center of the disc and on the debris-cloud center line. A central fragment was observed in all debris clouds where the t/D ratio was less than 0.2, and was most clearly observed in the late-time view of the debris cloud. This central fragment represented the most severe threat to rear wall integrity (Piekutowski, 1992a). The rear element of the structure is a hemispherical shell of fragments spalled from the rear surface of the sphere. The internal structure of the debris cloud, shown in Fig. 2 and subsequent figures, is the most significant feature of the debris cloud in terms of potential for rear wall damage. In the remainder of this paper, the term "debris cloud" will be considered synonymous with "internal structure."

The effect of a change in the t/D ratio on the debris-cloud morphology is shown in Fig. 3 for eight t/D ratios. All debris clouds shown in this figure were produced by the impact of a 9.53-mm-diameter 2017-T4 aluminum sphere with a 6061-T6 aluminum bumper at an impact velocity of 6.70 km/s $\pm$ 0.08 km/s. Use of other bumper materials, 1100-O and 2024-T3 aluminum, did not measurably affect debris-cloud shape or characteristics. As shown in Fig. 3, t/D ratios for the tests ranged from 0.026 to 0.424. As the t/D ratio increased from the minimum value, significant expansion of the internal structure of the debris cloud was observed. The following changes in internal-structure morphology occurred as t/D ratio increased: (1) the diameter of the disc-like

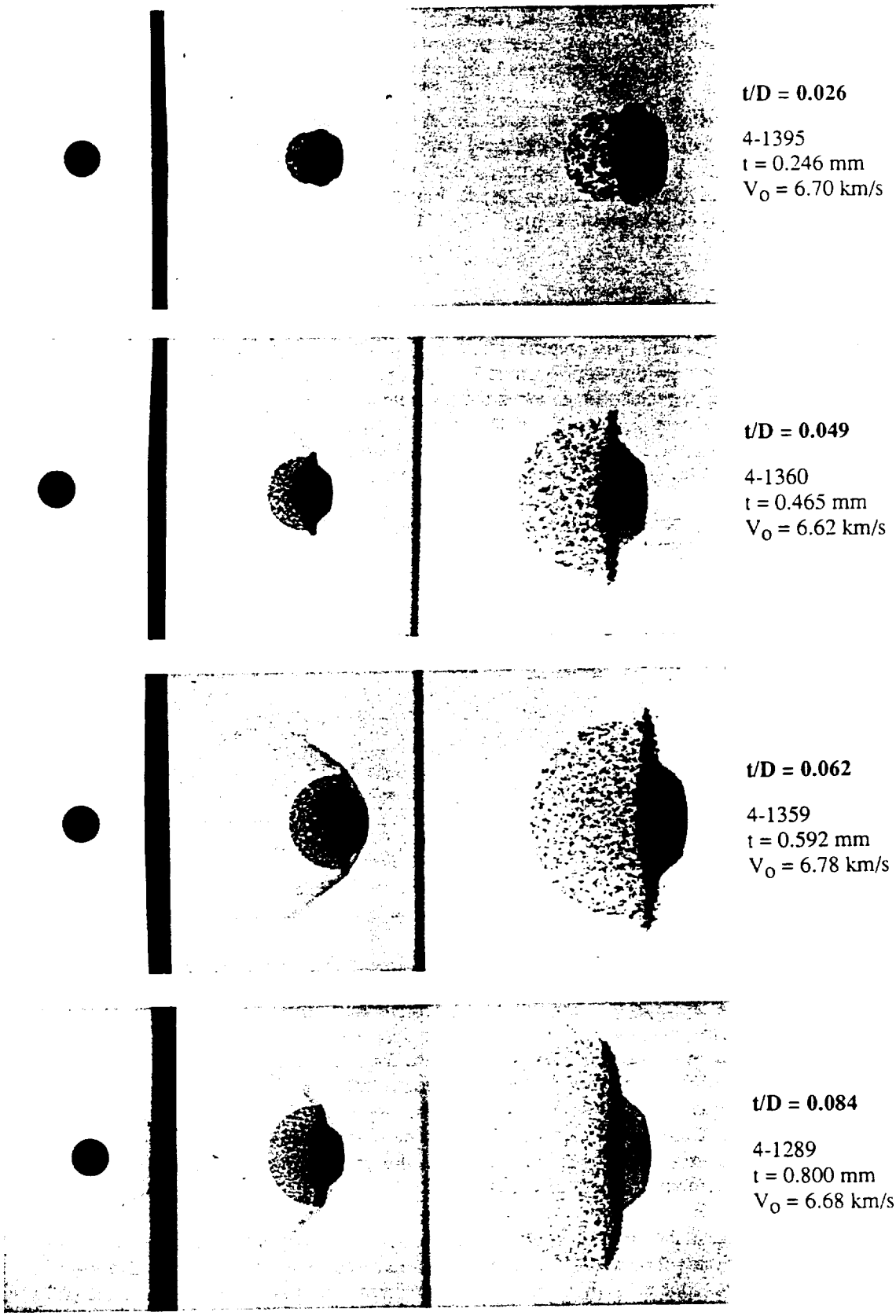

Fig. 3. Views of debris clouds produced by impact of 9.53-mm-diameter, 1.275-g, 2017-T4 aluminum spheres with various thicknesses of 6061-T6 aluminum plates. Impact velocity constant.

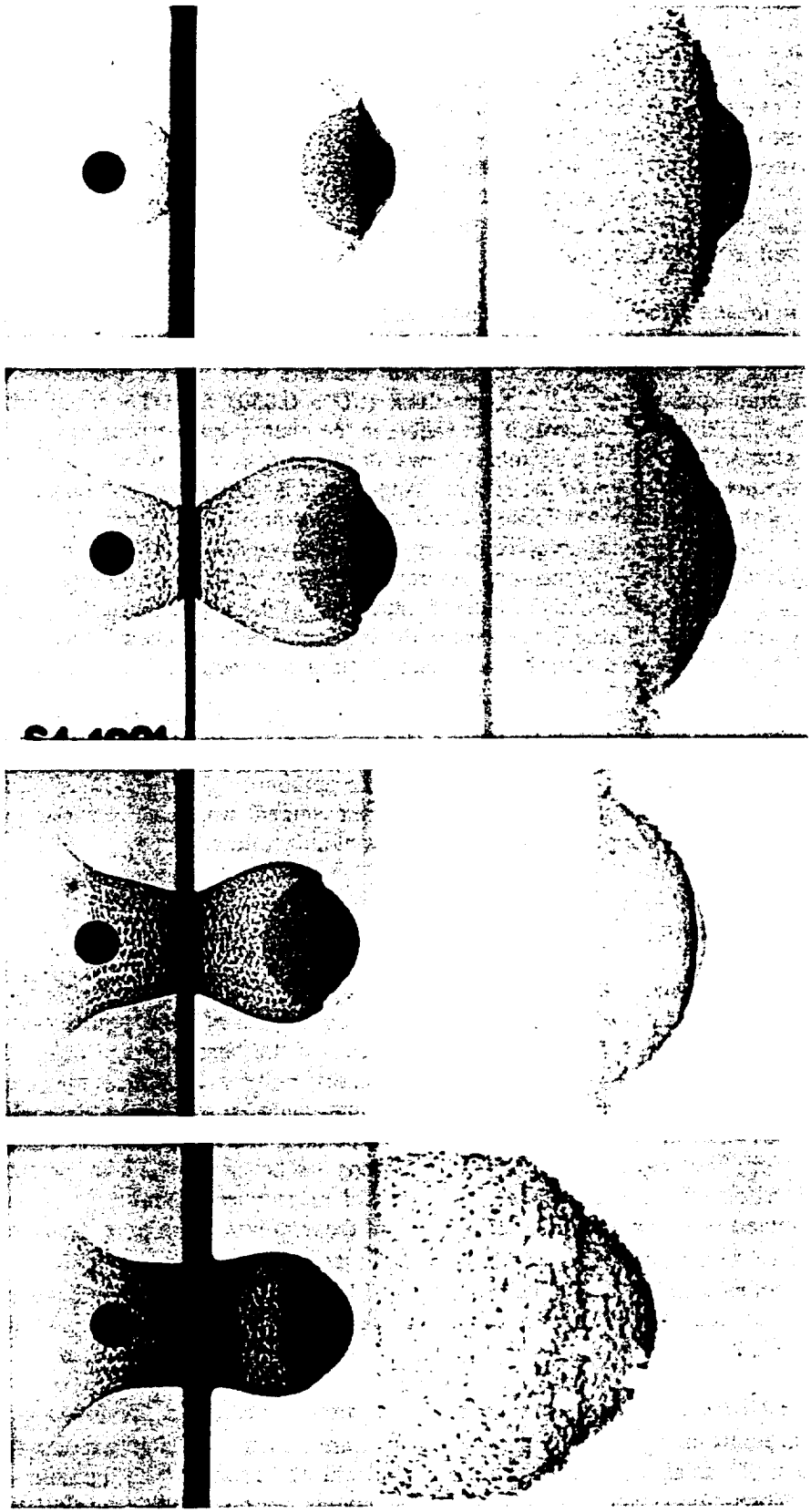

t/D = 0.102

4-1283
t = 0.968 mm
V_o = 6.72 km/s

t/D = 0.163

4-1291
t = 1.549 mm
V_o = 6.71 km/s

t/D = 0.234

4-1352
t = 2.225 mm
V_o = 6.64 km/s

t/D = 0.424

4-1353
t = 4.039 mm
V_o = 6.68 km/s

Fig. 3. (Concluded). Views of debris clouds produced by impact of 9.53-mm-diameter, 1.275-g, 2017-T4 aluminum spheres with various thicknesses of 6061-T6 aluminum plate. Impact velocity constant.

center element increased, began to "bend over" at a t/D of 0.084, and formed a flat-bottomed bowl at t/D = 0.163; (2) radial expansion of the hemispherical shell of spall fragments at the rear of the internal structure increased; and (3) the size of fragments in the center and rear element decreased. In contrast to the growth of the center and rear element, the front element of the cloud did not vary significantly in size, shape (a truncated cone), or radiographic density until the t/D ratio was greater than 0.102. At t/D ratios of 0.163 and 0.234 this element was a spherical sector and did not exist when the t/D ratio was 0.424. The relatively constant radiographic density of the front element for the lower t/D ratios was noteworthy when compared to the varying density of the external bubble of debris and the ejecta veil for these same tests.

The effects of a change in impact velocity on debris-cloud morphology are shown in Fig. 4 for tests with a constant t/D ratio. For the four lower velocity tests, 9.53-mm-diameter 2017-T4 aluminum spheres and 0.465-mm-thick (t/D = 0.049) 6061-T6 aluminum bumpers were used. A 6.35-mm-diameter 2017-T4 aluminum sphere and a 0.318-mm-thick (t/D = 0.050) 6061-T6 aluminum bumper were used for the 7.23 km/s test. Although not visible in the photographic reproduction of the radiograph for the test at 3.77 km/s, the post impact views for this test show a narrow region of reduced density just inside the rear surface of the sphere. Apparently, a spalled region developed inside the projectile, forming a shell that was loosely attached to the rear of the sphere. A slight flattening of the front of the sphere and a small piece of bumper that moved downrange of the front of the flattened sphere was also observed for this test. As impact velocity increased, fragmentation of the projectile and an increase in the axial and diametral expansion of the internal structure was observed. A small front element was clearly evident when the impact velocity reached 5.45 km/s. Further development of the front element occurred as impact velocity was increased to 6.62 km/s and 7.23 km/s.

Growth of the internal structure of a debris cloud was sensitive to both t/D ratio and impact velocity, and increased as both parameters increased--at least to the optimum t/D ratio (estimated to be between 0.18 and 0.20). Development and growth of the front element was most sensitive to impact velocity. Further quantitative comparisons of these debris-clouds follow.

RESULTS AND DISCUSSION

Readily identifiable points or locations in the debris clouds were assigned positions as shown by the circled numbers in Fig. 5. Axial and radial positions and velocities of each of these points, with respect to the cloud center line, and the radial expansion velocity of the hemispherical shell of projectile spall fragments was determined. Use of the fine-source, soft x-rays and a direct-exposure film produced radiographs in which fragments as small as 0.25 mm could be seen and measured. Accurate positioning of the heads and use of a common reference point, for all measurements taken from the radiographs, permitted specific debris-cloud positions to be determined to within $\pm$0.25 mm or better. Rotation of individual fragments at critical measurement points produced most of the error encountered when determining the location of these points. The time between firing of the pairs of flash x-rays was determined within $\pm$0.1 μs. Accordingly, velocities of material at measurement points could be determined to within $\pm$0.1 km/s or better. For those cases in which test results for two nearly identical test conditions were available, agreement between measured values was excellent.

Before examination of test results begins, several comments regarding notation in the following figures are in order. Six points in Fig. 5, ⑤ through ⑩ inclusive, are points for which two sets of measurements were taken; (1) axial distance from the bumper and (2) distance between points, measured normal to the debris-cloud center line. These measurements were used, with appropriate timing information, to determine axial and diametral velocities of these points or pairs of points, respectively. Axial velocities are denoted when the points are separated by a comma. Diametral velocities are denoted when the points are separated by a dash. All velocity data have been normalized by dividing specific measured velocities by the impact velocity used for the test.

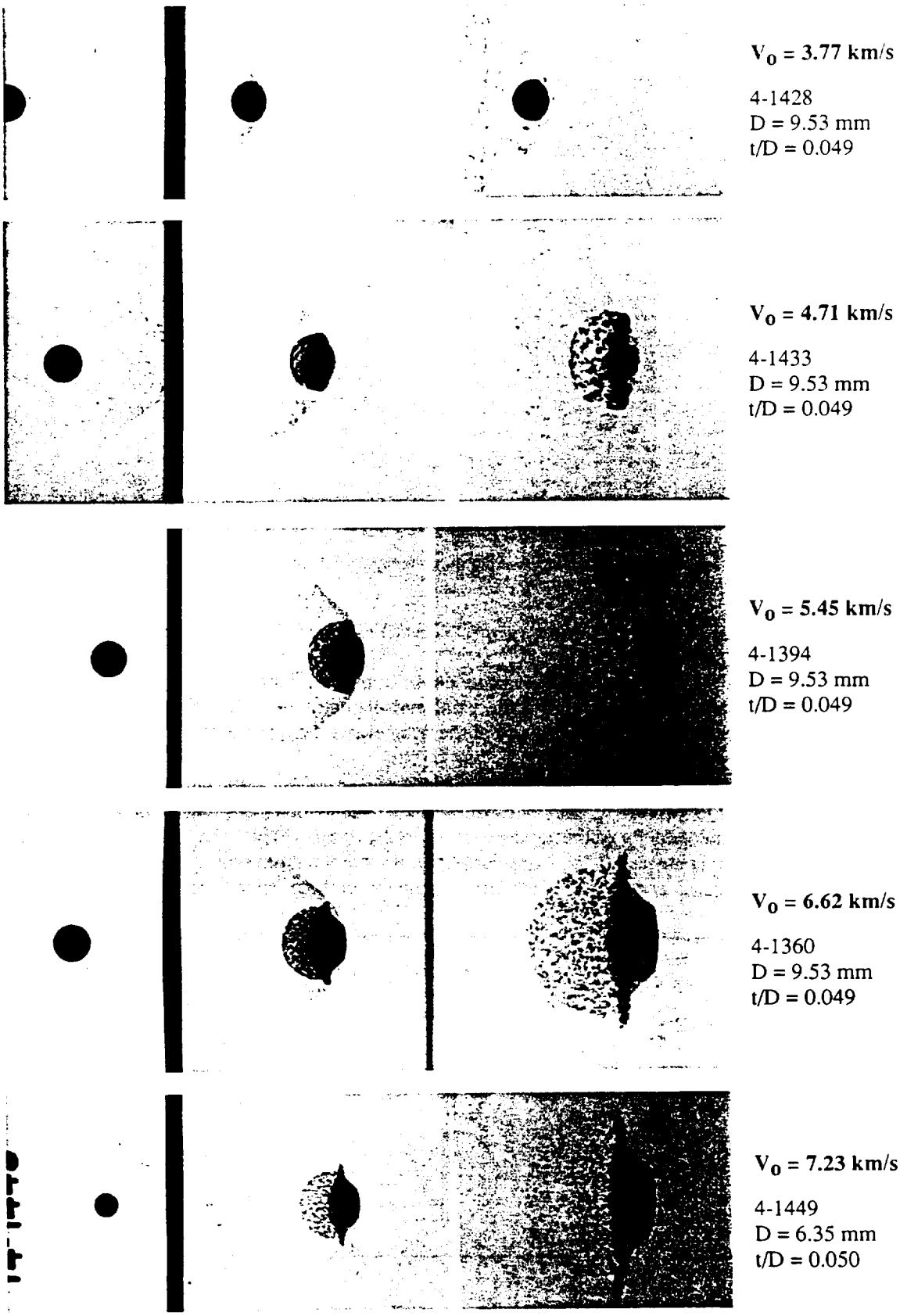

Fig. 4. Views of debris clouds produced by impact of 9.53-mm and 6.35-mm-diameter 2017-T4 aluminum spheres with 6061-T6 aluminum plates. Impact velocity varied and t/D ratio held constant.

Fig 5. Points used when making measurements of debris-cloud features.

Effect of t/D Ratio and Impact Velocity on Debris-Cloud Velocities

In this section, the effects of a change in t/D ratio and/or impact velocity on the velocity of the axial measurement points of the debris cloud, the axial and diametral velocity of the center disc-like element, and the axial and diametral velocity of the front element are presented, in that order.

In Fig. 6a, normalized axial debris-cloud velocities decrease as t/D ratio increases. Overall, an increase in the axial dispersion of the cloud is observed. The velocity of point ② is probably very close to or may be the velocity of the center of mass of the debris cloud. The observed decrease in velocity of this point is not surprising since conservation of momentum would predict this behavior as the t/D ratio increases and the mass of bumper involved in the collision increases. The velocity

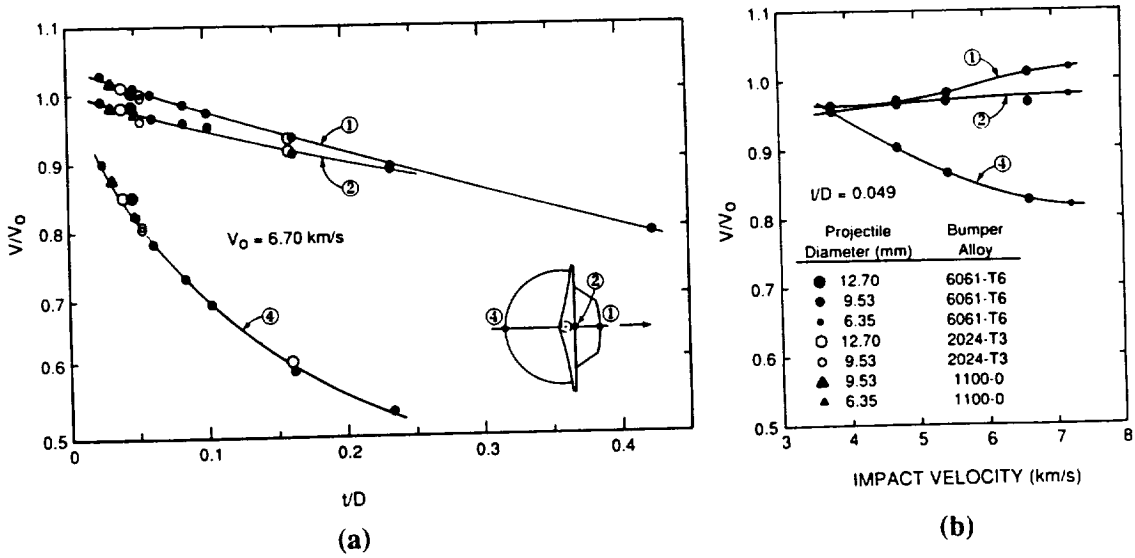

Fig. 6. Normalized velocity of selected on-axis measurement points in debris cloud versus t/D ratio and impact velocity.

of point ② in Fig. 6b is nearly constant, as would be expected since the t/D ratio is constant. However, the sudden increase in velocity of point ① in Fig. 6b is noteworthy and will be discussed in more detail later in this section. The velocity of point ④, in Fig. 6b, appears to be approaching the value shown for a t/D of 0.049 in Fig. 6a.

Normalized axial and diametral velocities of points ⑨ and ⑩ are shown in Fig. 7. A decrease in axial velocity and an increase in the diametral velocity of these points occurs as the t/D ratio increases. These points cease to be distinct in the cloud when the t/D ratio is between 0.10 and 0.16 because of rearward flow at the periphery of the center element. As impact velocity increases, little change in the axial velocity of this region is observed; however, a moderate increase of the diametral velocity of these points occurs.

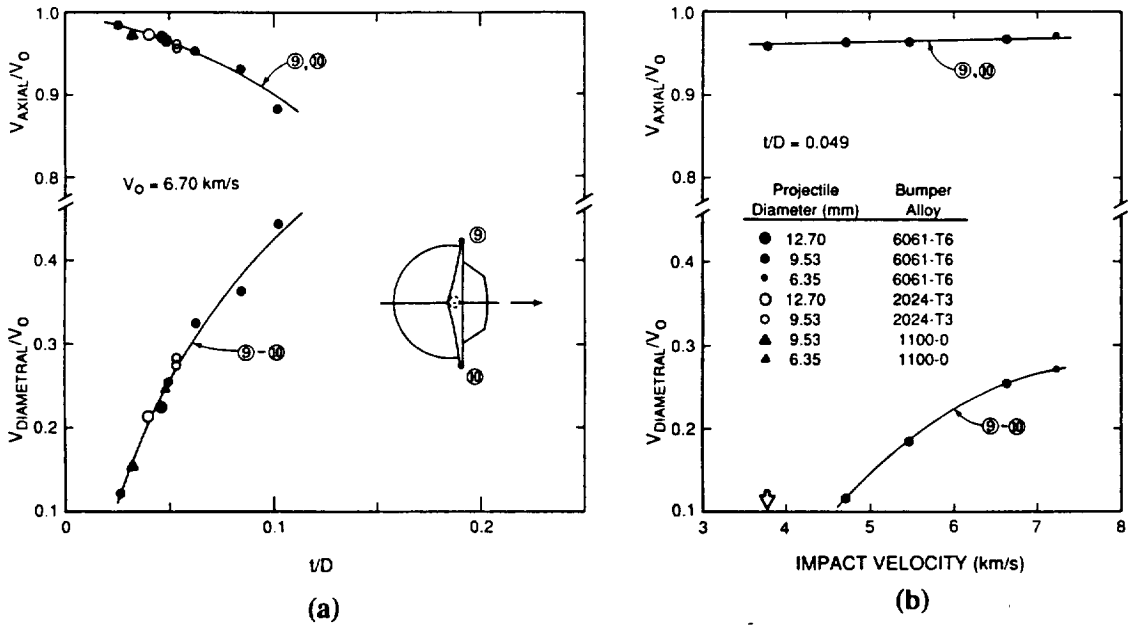

Fig. 7. Normalized axial and diametral velocities of center element of debris cloud versus t/D ratio and impact velocity.

Normalized axial and diametral velocities of points ⑤, ⑥, ⑦, and ⑧ are presented in Fig. 8. As t/D ratio increases, in Fig. 8a, the axial velocity of all four points decreases. Points ⑤ and ⑥ cease to be distinct when this element changes from a truncated-cone shape to a spherical sector at a t/D ratio between 0.10 and 0.16. The diametral velocity of these pairs of points increases slightly to a maximum at t/D = 0.16, then decreases rapidly until this feature disappears (t/D > 0.23). The opposite behavior of these points is observed when impact velocity increases. The axial velocity of points ⑤ and ⑥ increases considerably; however, little or no change in the axial velocity of points ⑦ and ⑧ is observed. Significant increases in the diametral velocity of both pairs of points, particularly ⑦ and ⑧, are the most noteable feature of Fig. 8b.

Growth of the debris-cloud internal structure occurs as t/D ratio and impact velocity increase. Comparison of normalized debris-cloud velocities, as a function of t/D ratio, indicates that the velocities of points used to evaluate this growth agree (within measurement limits) despite a factor of two variation in projectile diameter and a factor of eight in projectile mass. The limited data (one point) would indicate that similar agreement of normalized velocities occurs as impact velocity is varied. Caution is urged in extending these observations to all combinations of t/D ratio and impact velocity, however. The development and growth (or minimal growth) of the front element was the most interesting and significant aspect of comparison of debris-cloud features.

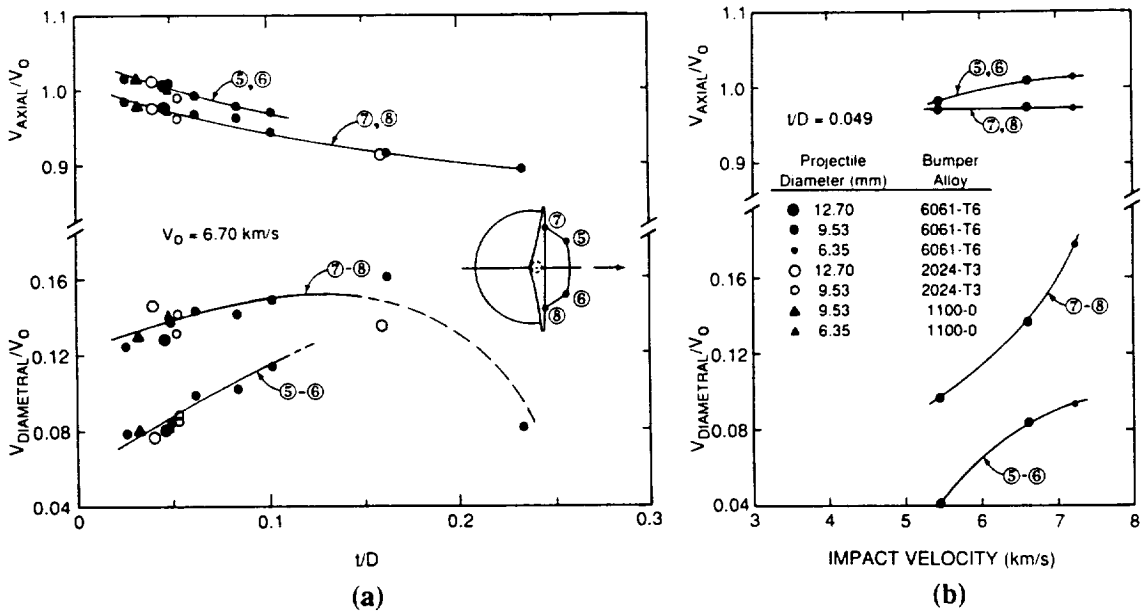

Fig. 8. Normalized axial and diametral velocities of front element of debris cloud versus t/D ratio and impact velocity.

Model for Early-Time Interactions at Impact Site

Late-time views of the debris clouds presented in Fig. 4 are shown in Fig. 9. These late-time views clearly show the development and growth of the front element of the debris-cloud internal structure as impact velocity increases. The front element of each view in Fig. 9 consists of the following: (9a) and (9b) a single fragment and several solid fragments, respectively; (9c) a small cloud of solid fragments; (9d) and (9e) a large cloud of finely divided droplets of molten aluminum.

A model for the formation of the front element is presented in this subsection. The essential features of the model are shown in Fig. 10. The model draws heavily on a description of the kinematics of the impact process given by Ang (1990) and used to determine the source of material

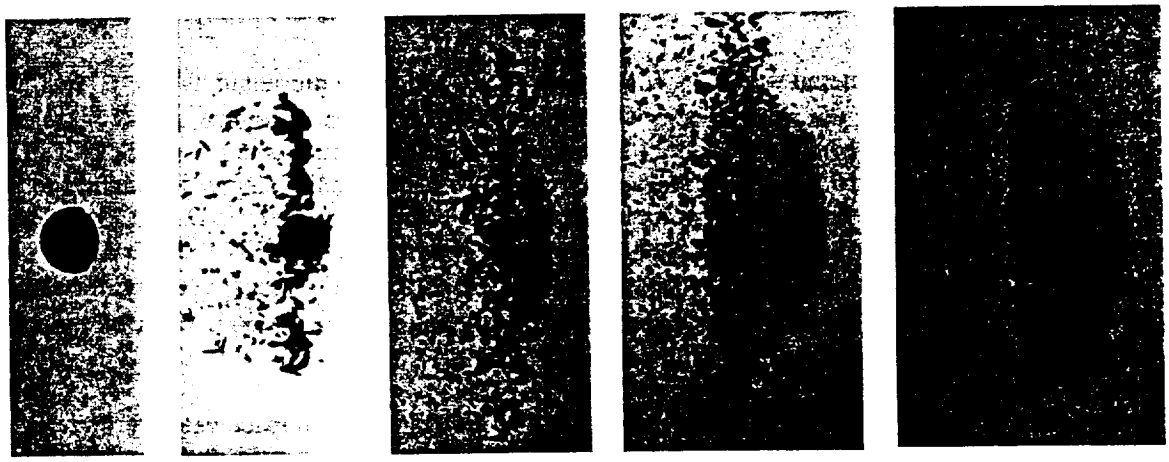

Fig. 9. Late-time views of debris clouds showing development of front element of internal structure as a function of increase in impact velocity. Views (a) through (d) used 9.53-mm-diameter, 2017-T4 aluminum spheres. View (e) used a 6.35 mm-diameter, 2017-T4 aluminum sphere. All tests used 6061-T6 aluminum bumpers (t/D = 0.049). See Fig. 4 for earlier views of these clouds.

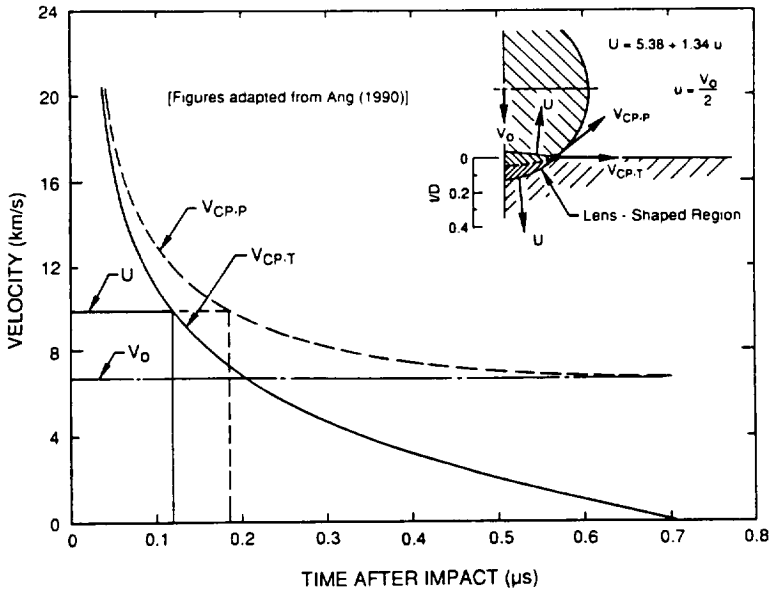

Fig. 10. Illustration of interactions at impact site. Collision-point velocities versus time after impact, for a 9.53-mm-diameter sphere traveling at 6.70 km/s, are shown in this figure. In the inset, the impacting sphere and impacted plate are shown with appropriate notation for the velocities referenced in the paper.

dominating an impact flash signature. In Fig. 10, U is the shock-wave front velocity, u is the particle velocity behind the shock-wave front, V_0 is the sphere impact velocity, $V_{CP,P}$ is the velocity of the collision point between the surfaces of the sphere and target in the reference frame of the projectile, and $V_{CP,T}$ is the velocity of the collision point in the reference frame of the target. Half of a sphere impacting half a semi-infinite plate is shown in the inset in this figure.

As shown in Fig. 10, $V_{CP,\,T}$ is greater than U for the first 0.12 μs after impact. Consequently, loading of the lens-shaped region shown in the inset is quasi one-dimensional during this time interval. Formation of release waves at the boundaries of the lens-shaped region is not possible as long as $V_{CP,\,T}$ is greater than U. When $V_{CP,\,T}$ is less than U, release waves are generated in the target prior to contact by the oncoming sphere. As the impact process continues, formation of release waves in the sphere begins and a decrease in U occurs, due to spherical divergence of the wave front. These later-time events quickly complicate description of the shock-wave interactions taking place during the remainder of the impact event. In the inset in Fig. 10, the lens-shaped region of compressed material is shown to scale at the time $V_{CP,\,T}$ equals U (0.12 μs after impact). The diameter of the compressed region is approximately 59 percent of the diameter of the sphere. Also shown is a t/D scale that allows the reader to determine the fraction of bumper-plate thickness that experiences quasi one-dimensional loading during impact.

The nearly constant radiographic density and shape of the front element, for the low t/D ratio tests, would indicate that the materials involved in the formation of the front elements experienced similar shock loadings. At greater t/D ratios, increasingly larger volumes of material are involved in formation of the front elements. However, this material is derived from regions where the shock wave interactions are complicated and where shock-wave velocities and pressures are lower. These factors contribute to processes that alter the prominence and shape of the front element.

Growth of the lens-shaped region, shown in Fig. 10, into the darker portion of the front element is illustrated in Fig. 11a. The diameter of the heavily shaded region in this figure was determined from the radiograph of the debris cloud shown in Fig. 11b. This diameter and the measured diametral velocity of this portion of the debris cloud were used to compute the diameter of the lens-shaped region at 0.12 μs after impact. The computed diameter and the nominal diameter of this region (59 percent of the sphere diameter) agreed exactly. The darker region in the front element was also observed in radiographs of tests with t/D ratios of 0.026 and 0.049.

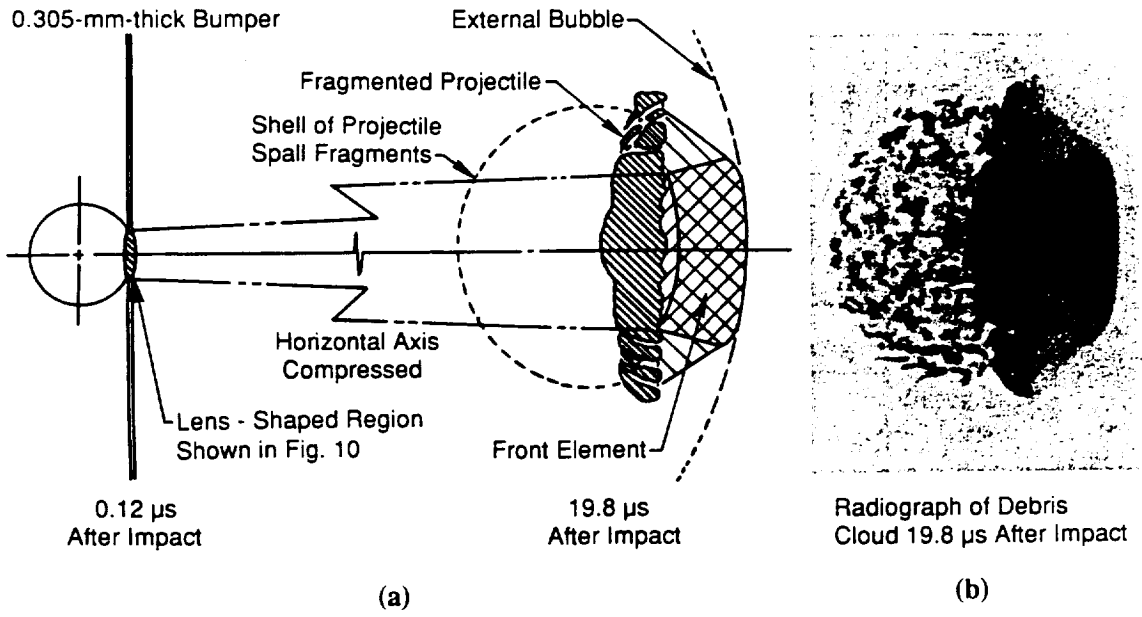

Fig. 11. Development of features in front element of internal structure of debris cloud. (a) Expansion of region in which collision-point velocity in target exceeds shock-wave front velocity (see Fig. 10). (b) View of debris cloud produced by impact of a 9.53-mm-diameter 2017-T4 aluminum sphere with an 1100-O aluminum sheet at 6.67 km/s (Shot 4-1290, t/D = 0.032).

Effect of Change of State on Debris-Cloud Velocities and Morphology.

Projectile and bumper-plate material that form the front element are the most intensely shocked material in the debris cloud. It has been shown (see Anderson et al., 1990, for example) that release from a shocked state is a nearly isentropic process and that a significant amount of energy remains in the previously shocked material after release. This residual energy is converted to heat and, depending on the amount of heat available, melting and/or vaporization of the previously shocked material may occur. Anderson et al. have estimated the residual temperatures, as a function of particle velocity of the shocked material, for four metals: aluminum, cadmium, lead, and molybdenum. An adaptation of a figure taken from their work is presented in Fig. 12 and shows the results of their computations for aluminum. The lens-shaped region of Fig. 10 can be

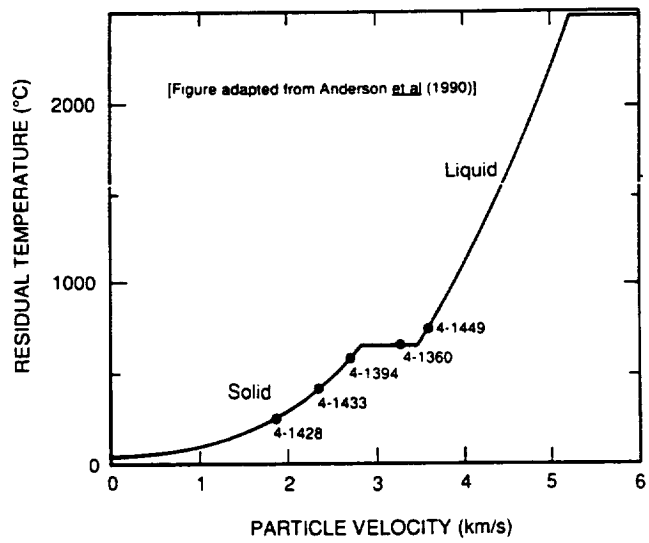

Fig. 12. Estimated residual temperature versus particle velocity using Tillotson EOS. Shot numbers shown in this figure are for tests discussed in text.

treated as experiencing a nearly one-dimensional shock. Following release from the shocked state, material in this region should attain temperatures and phases indicated in Fig. 12. As the t/D ratio increases, material outside this region would not be as highly shocked and increasingly larger portions of the bumper and projectile would remain as solid but heated fragments.

Studies performed at UDRI, by Schmidt et al. (1993), have provided radiographs of tests in which cadmium spheres were fired at cadmium plates (t/D ratios ~ 0.16). Impact velocities for these tests were high enough to cause vaporization of projectile and bumper material. Results of an analysis of these tests and the tests with aluminum spheres and plates were used to develop the sequence of debris-cloud cross sections illustrated in Fig. 13. In this figure, effects of change of state due to increased impact velocity are first manifested in the lens-shaped region shown in Figs. 10 and 11. When impact velocity is low, the cloud is composed of solid fragments. As impact velocity increases, a small region of liquid develops but may have a thin zone of solid-liquid phase bumper material at the front and a thick zone of solid-liquid phase projectile material at the rear. The entire zone liquefies as impact velocity and residual temperature increases. Further increases in impact velocity produce regions of liquid-vapor phase and vapor. Low-density vaporous material at the front of the cloud is driven outward due to the expansion of regions of higher density vapor below. This outward expansion produces a fuller and more rounded debris-cloud profile. As expansion continues, the regions of high-density vapor are exhausted and disappear. The increase in the velocity of point ②, in Fig. 6b, is indicative of a significant decrease in material strength resulting from complete liquefaction of material in the front element.

Similarities between the cadmium and aluminum debris cloud were striking when the comparisons were made on the basis of t/D ratio. In Schmidt et.al., issues related to scaling of impact velocity, thermodynamic properties of the materials involved in the impact, etc., are discussed. Test results presented by Schmidt et.al. show that properly scaled aluminum and cadmium experiments produced similar damage to or failure of the rear wall of a Whipple-type shield. Similarity of cloud structure and properties has been observed in the other UDRI tests involving impacts of like materials. The structural features of the aluminum tests described in this paper conform to the features shown for the low and moderate impact velocity debris clouds in Fig. 13. All evidence indicates that impacts of aluminum spheres with aluminum plates at velocities high enough to produce vaporization would produce debris clouds that look like the vaporous cloud shown in Fig. 13.

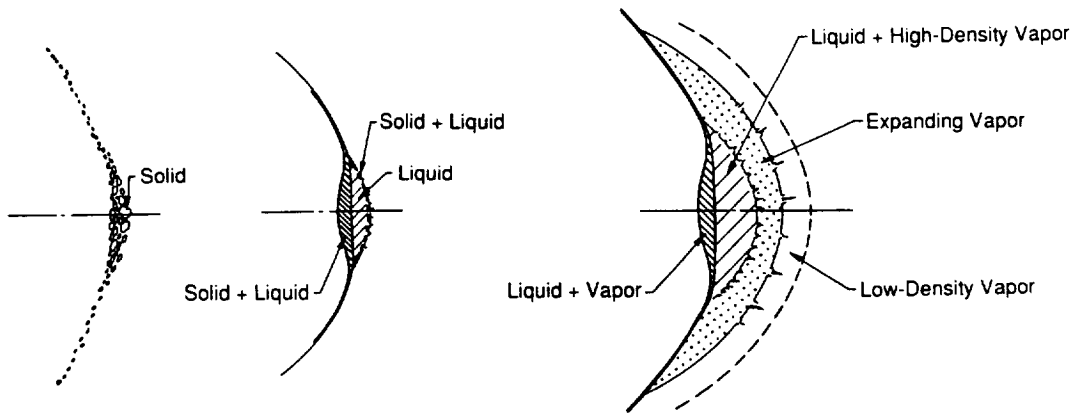

Fig. 13. Illustration of various debris-cloud structural features resulting from change of phase of material in cloud elements. Cloud development typical for t/D ratio near or just below optimum.

SUMMARY

Debris clouds produced by the impact of aluminum spheres with thin aluminum plates were shown to consist of three structural features: (1) an ejecta veil, (2) an external bubble of debris, and (3) a significant structure inside the external bubble of debris. The internal structure consisted of a front,

center, and rear element. The prominence and size of the three internal structural elements was shown to vary with t/D ratio and impact velocity. Changes in impact velocity produced the more significant changes in the front element.

A model for the development of the front element of the internal structure was presented. This model and the appropriate thermodynamic descriptions of the metals used for the bumper and projectile can be used to determine the state of material in this region of the debris cloud. A description of a debris cloud containing solid, solid-liquid, and/or liquid-vapor phases was presented.

ACKNOWLEDGMENT

A major portion of the analytical effort and several of the tests were performed under Prime Contract NAS 8-38856 on Subcontract A71447 with Martin Marietta Manned Space Systems (MMMSS). The author wishes to gratefully acknowledge Mr. Joel Williamsen, NASA MSFC and Dr. Norman Elfer (MMMSS) for their support of this work. He also wishes to express his appreciation to Mr. Burton Cour-Palais of McDonnell Douglas Space Systems Company and Dr. Robert Schmidt of Boeing Defense & Space Group for the use of their data and to Dr. Schmidt for providing several of the thinner 6061-T6 bumper-sheet materials used in the tests.

The author would also like to express his appreciation to the following associates at UDRI: The Office of the Director, for support provided for the range and equipment tests; Kevin Poormon and Donald Jurick, for their many helpful discussions; Robert Gooding and Chuck Blair, for performing the test firings; Richard Tocci and Brian Oesgher, for their careful handling and printing of the radiographs; and Gloria Hardy and Kristy Johnson, for their patience and care in preparing the manuscript.

REFERENCES

Anderson, C.E., T.J. Trucano, and S.A. Mullin (1990). Debris Cloud Dynamics. Int. J. Impact Engng, **9**, No. 1, pp. 89-113.

Ang, J.A. (1990). Impact Flash Jet Initiation Phenomenology. Int. J. Impact Engng, **10**, pp. 23-33.

Backman, M.E. and W.J. Stronge (1967). Penetration Mechanics and Post-Perforation Effects in an Aluminum-Aluminum System. NWC TP 4414.

Maiden, C.J. (1963). Experimental and Theoretical Results Concerning the Protective Ability of a Thin Shield Against Hypervelocity Projectiles. Proc. 6th Symp. on Hypervelocity Impact. Cleveland, OH, Vol. 3, 69.

Maiden, C.J., A. R. McMillan, and R.E. Sennett (1965). Thin Sheet Impact, NASA CR-295.

Nysmith, C.R. and B.P. Denardo (1969). Experimental Investigation of the Momentum Transfer Associated with Impact into Thin Aluminum Targets. NASA TN D-5492.

Piekutowski, A.J. (1992a). Properties of Largest Fragment Produced by Hypervelocity Impact of Aluminum Spheres with Thin Aluminum Sheets. Proc. AIAA Space Programs and Technologies Conference. Huntsville, AL, Paper No. 92-1588.

Piekutowski, A.J. (1992b). Formation and Description of Debris Clouds and Related Damage to Shield Structures Resulting from Hypervelocity Impact. UDR-TR-92-128, to be published as a NASA contractors report. Marshall Space Flight Center, AL.

Schmidt, R.M., K.R. Housen, A.J. Piekutowski, and K.L. Poormon (1993). Cadmium Simulations of Orbital Debris Shield Performance to 18 km/s. Int. J. Impact Engng, **14**.

Swift, H.F. and A.K. Hopkins (1968). The Effects of Bumper Material Properties on the Operation of Spaced Hypervelocity Particle Shields, AFML-TR-68-257.